



Published in final edited form as:

Anal Chem. 2011 November 1; 83(21): 8158–8168. doi:10.1021/ac201658s.

Theoretical Design and Analysis of Multivolume Digital Assays with Wide Dynamic Range Validated Experimentally with Microfluidic Digital PCR

Jason E. Kreutz^a, Todd Munson^b, Toan Huynh^a, Feng Shen^{a,†}, Wenbin Du^{a,‡}, and Rustem F. Ismagilov^{a,*,§}

^aDepartment of Chemistry and Institute for Biophysical Dynamics, The University of Chicago, 929, East. 57th St., Chicago, Illinois 60637

^bUniversity of Chicago, Computation Institute, Chicago, IL 60637 USA and Argonne Natl Lab, Argonne, IL 60439 USA

Abstract

This paper presents a protocol using theoretical methods and free software to design and analyze multivolume digital PCR (MV digital PCR) devices; the theory and software are also applicable to design and analysis of dilution series in digital PCR. MV digital PCR minimizes the total number of wells required for “digital” (single molecule) measurements while maintaining high dynamic range and high resolution. In some examples, multivolume designs with fewer than 200 total wells are predicted to provide dynamic range with 5-fold resolution similar to that of single-volume designs requiring 12,000 wells. Mathematical techniques were utilized and expanded to maximize the information obtained from each experiment and to quantify performance of devices, and were experimentally validated using the SlipChip platform. MV digital PCR was demonstrated to perform reliably, and results from wells of different volumes agreed with one another. No artifacts due to different surface-to-volume ratios were observed, and single molecule amplification in volumes ranging from 1 to 125 nL was self-consistent. The device presented here was designed to meet the testing requirements for measuring clinically-relevant levels of HIV viral load at the point-of-care (in plasma, <500 molecules/mL to >1,000,000 molecules/mL), and the predicted resolution and dynamic range was experimentally validated using a control sequence of DNA. This approach simplifies digital PCR experiments, saves space and thus enables multiplexing by using separate areas for each sample on one chip, and facilitates the development of new high-performance diagnostic tools for resource-limited applications. The theory and software presented here are general, and are applicable to designing and analyzing other digital analytical platforms including digital immunoassays and digital bacterial analysis. It is not limited to SlipChip, and could also be useful for the design of systems on platforms including valve-based and droplet-based platforms. In the accompanying paper by Shen et al. (*JACS* 2011), this approach is used to design and test digital RT-PCT devices for quantifying RNA.

rustem.admin@caltech.edu.

[†]Current Address: SlipChip, LLC, 2201 Campbell Park Drive, Chicago, IL, 60612

[‡]Current Address: Department of Chemistry, Renmin University of China, Beijing, China, 100872

[§]Current Address: Division of Chemistry and Chemical Engineering, California Institute of Technology, 1200 E. California Blvd, Pasadena, CA 91125.

Supporting Information Available: Chemicals and materials, detailed experimental procedures, additional tables, computer software, and complete references (4) and (36). This material is available free of charge via the Internet at <http://pubs.acs.org>

Disclosure: F.S. and R.F.I. have a financial interest in SlipChip LLC.

Introduction

This paper presents a theory and an experimental validation for design and analysis of digital PCR devices that rely on multiple sets of wells, each set of a different volume. We also present design principles to develop user-specified devices. This approach, defined here as “Multivolume digital PCR” (MV digital PCR), enables quantification of nucleic acid with wide dynamic range and high resolution while using a minimal number of wells.

The development of simple stand-alone devices for quantitative nucleic acid diagnostics would further enable diagnosis and treatment in point-of-care settings. Precise, absolute quantification of nucleic acid levels, especially at low levels of detection, would have particular impact in applications such as viral load analysis (e.g. HIV, Hepatitis, Cytomegalovirus (CMV), enterovirus),^{1–12} bacterial detection and quantification in food or water sources without culturing,^{13–15} multiplexed diagnostics, and minimal residual disease.^{16,17} Real time PCR is often considered the gold standard for nucleic acid quantification,^{18–20} but has limited utility in the field because it requires data collection and analysis over the entire course of the reaction, careful control of conditions, and internal calibration standards, and typically gives relative levels rather than absolute concentrations.^{9,21–23} Digital PCR^{23–41} provides a way to obtain absolute nucleic acid levels directly using only endpoint analysis with high resolution and sensitivity.

Typical digital PCR platforms^{25–32} use wells of only a single volume, and therefore require a large number of wells to achieve a large dynamic range. In single-volume digital PCR, the upper limit of quantification (ULQ) is determined predominantly by the volume of individual wells; the number of wells also contributes to the upper limit. The lower detection limit (LDL) is determined by the total volume, thus a large dynamic range requires tens of thousands to millions of small wells. While acceptable in standard laboratory settings, this is a potential limitation for point-of-care purposes, which would benefit from fewer wells to make chip design and readout more manageable and minimize device footprint. In addition, in single volume approaches, resolution and dynamic range cannot be adjusted independently, regardless of the actual requirements of a given application, leading to inefficient experimental design.

Serial dilutions have been used in digital PCR systems^{23–29,31–33} to expand the dynamic range, but this approach only expands the dynamic range to higher concentrations and does not increase sensitivity. Most digital PCR systems use wells with small (few nL or pL) volumes, making quantification of low concentrations (~100 molecules/mL) difficult. Digital PCR in wells with larger volumes combined with serial dilution can be used to quantify low and high concentrations, but this approach would waste both space and reagent. Using serial dilutions increases sample manipulation and processing, adds complexity, and increases the potential for cross-contamination, making it less applicable in point-of-care settings.

MV digital PCR overcomes these limitations of serial dilutions and allows the user to quantify nucleic acid while adjusting dynamic range and resolution separately (Figure 1a). Wells of different volumes decouple the link between the total volume of all wells and the size and number of smallest wells: the smallest wells enable quantification of high concentrations, while the wells of large volumes enable high sensitivity by efficiently increasing the total volume. MV digital PCR can achieve the same dynamic range as single-volume digital PCR without the need for an excessive number of wells (compare Figure 1b and 1c, or Figure S1a and S1b). By reducing the number of wells required for a given dynamic range, more samples can be tested on a single chip, allowing for multiplexed

testing. The MV system also requires less reagent (>67% less for the design described in this paper) than serial dilution, thus reducing cost.

A key feature of the approach in this paper is the mathematical treatment for combining of results from multiple volumes. While the use of multiple volumes can be mathematically equivalent to using serial dilutions, most work in this area has treated each dilution separately.^{23–29,33} Combining results from wells of multiple volumes increases accuracy and can be achieved using the maximum likelihood estimate (MLE), or Most Probable Number (MPN) theory^{42–49} as it is known in culture-based bacterial quantification systems. Three replicates (i.e. wells) at three dilutions has long been the standard for this method, though it has been expanded to include increased numbers of wells to improve quantification using multivolume approaches.^{47–49} Such a “three replicates at three dilutions” approach has been used to perform “MPN-PCR” based quantification,^{13–15} although current digital PCR systems^{25–32} have used only elements of MPN for analysis^{31,32} of serial dilution experiments. Microfluidic devices for multivolume digital PCR, and appropriate statistical methods for proper analysis, have not been previously developed.

Here, we wished to expand and test the MPN theory in the context of multivolume digital PCR. We also wished to perform experimental tests of this approach because it was not obvious that digital PCR would function properly at all well volumes due to the potential artifacts caused by different surface-to-volume ratios and different effective concentrations of single molecules in each volume. The SlipChip^{31,50–56} is an attractive platform for this multivolume approach, as it can easily incorporate wells of different sizes. The simplicity of the device (e.g. lack of valves and pumps and control channels) allowed for the design of nonlinear (e.g. radial) arrays to further reduce the footprint of the device. We chose to validate the MV digital PCR approach by designing a SlipChip device that meets the detection requirements to monitor HIV viral load. An ideal diagnostic tool to measure HIV viral load would have a wide dynamic range to measure 500 to 1,000,000 molecules/mL in plasma while achieving a resolution of 3-fold changes (0.5 log) in viral load at a confidence level of at least 95% with a power level of 95%.^{1–7}

Here, we validated the design and the MV digital PCR approach using a control DNA template; in the accompanying paper we show that MV digital RT-PCR can also be performed for RNA using the design and analysis techniques provided here.⁵⁵ To apply MV digital nucleic acid quantification to point-of-care settings, digital isothermal amplification methods^{56–58} and visual readout methods will also be desired, but MV digital PCR provides an excellent starting platform to achieve this ultimate goal.

Experimental Section

Materials, DNA template preparation, and MV digital PCR experiments are described in the Experimental Section of the Supporting Information (SI).

Computer programs

The suite of programs developed in this work are provided in the SI (MVdPCR_Final_Programming_Code.zip) along with detailed descriptions. The user inputs the data into Datainput.xls and needs to interact with MVdPCR_DataInput.m; MVdPCR_RunSim.m; MVdPCR_Find_device_param.m; and MVdPCR_RunPlot.m programs. These programs would automatically execute additional programs provided in the suite: MVdPCR_MLE.m; MVdPCR_Simulate.m; MVdPCR_Find_device_resol.m; MVdPCR_Find_device_lower.m; MVdPCR_Find_approx1.m; and MVdPCR_Plot_points.m.

Results and Discussion

Poisson analysis of single-volume PCR

There are two key assumptions that need to be maintained in order for digital PCR methods and analysis to accurately quantify nucleic acid concentrations: 1) Having at least one target molecule in a well is necessary and sufficient for a positive signal and 2) Target molecules do not interact with one another or device surfaces, to avoid biasing their distribution. At the simplest level of analysis, when molecules are at low enough densities that there is either 0 or 1 molecule within a well, concentrations can be estimated simply by counting positives. However, if the two key assumptions above hold true, then Poisson and binomial statistics can be used to obtain quantitative results from experiments resulting in one positive well to experiments resulting in one negative well.^{59,60} The Poisson distribution (Eq. 1), in the context of digital PCR, gives the probability, p , that there are k target molecules in a given well based on an average concentration per well, $v \cdot \lambda$, where v is the well volume (mL) and λ is the bulk concentration (molecules/mL). In digital PCR, the same readout occurs for all $k > 0$, so if $k=0$ then Eq. 1 simplifies to give the probability, p , that a given well will not contain target molecules (the well is “negative”).

$$p = \left((v \cdot \lambda)^k \cdot e^{-(v \cdot \lambda)} \right) / k!, \text{ and for } k=0 \text{ (empty well), } p = e^{-(v \cdot \lambda)} \quad (1)$$

In single-volume systems, the number of negative wells, b , out of total wells, n , can serve as an estimate for p , so expected results can be estimated from known concentrations, or observed results can be used to calculate expected concentrations (Eq. 2).

$$b = n \cdot e^{-(v \cdot \lambda)} \text{ or } \lambda = -\ln(b/n)/v \quad (2)$$

The binomial equation is used to determine the probability, P , that a specific experimental result (with a specific number of negatives, b , and positives, $n-b$, out of the total number of

wells, n , at each volume) will be observed, based on λ (Eq. 3), where $\binom{n}{b} = \frac{n!}{b!(n-b)!}$.

$$P = \binom{n}{b} \cdot p^b \cdot (1-p)^{n-b} \text{ or } P = \binom{n}{b} \cdot (e^{-v \cdot \lambda})^b \cdot (1 - e^{-v \cdot \lambda})^{n-b} \quad (3)$$

Analysis of multivolume systems

Incomplete analysis of multivolume systems could be performed by simply selecting a single volume and analyzing it as described above; this is the approach that has typically been taken in serial dilution systems. The single volume that minimizes the standard error is generally chosen; this typically occurs when 10–40% of wells are negative.^{33,42,43} However this method wastes the information from the other “dilutions” (or volumes), and would require using different dilutions for different sample concentrations. Combining the results from wells of different volumes fully minimizes the standard error and provides high-quality analysis across a very large dynamic range. This is achieved by properly combining the results of multiple binomial distributions (one for each volume); specifically, the probability of a specific experimental result P (defined above) is the product of the binomials for each volume (Eq. 4),^{42–45} where P is defined as a function of the bulk concentration λ , $P = f(\lambda)$,

$$f(\lambda) = P = \prod \binom{n_i}{b_i} \cdot (e^{-v_i \cdot \lambda})^{b_i} \cdot (1 - e^{-v_i \cdot \lambda})^{n_i - b_i} \quad (4)$$

For a given set of results, the MPN is found by solving for the value of λ that maximizes P . In general taking the derivative of an equation and solving for zero provides the maximum and/or minimum values of that equation; as a binomial distribution (and subsequently the product of binomials) has only a single maximum, solving the derivative of Eq. 4 for zero provides the “most probable” concentration. The standard deviation, σ , is more appropriately applied to $\ln(\lambda)$ than to λ , because the distribution of P based on $\ln(\lambda)$ is more symmetrical than that for λ .^{42,43} In addition, this approach provides better accuracy for low concentrations by enforcing the constraint that concentrations must be positive. Thus a change of variables is needed during the derivations so σ can be found for $\ln(\lambda)$. Therefore, $f(\lambda)$ (Eq. 4) is converted to $F(\Lambda)$ (Eq. 5), where $\theta = e^{-v}$ and $\Lambda = \ln(\lambda)$

$$F(\Lambda) = P = \prod \binom{n_i}{b_i} \cdot (\theta_i^\Lambda)^{b_i} \cdot (1 - \theta_i^\Lambda)^{n_i - b_i} \quad (5)$$

The derivative is easier to handle if the natural log is applied to Eq. 5, as the individual components are separated, but the overall result is unchanged (Eq. 6).⁴³

$$L(\Lambda) = \ln F(\Lambda) = \sum_{i=1}^m \left(\ln \binom{n_i}{b_i} + b_i \cdot e^\Lambda \cdot \ln(\theta_i) + (n_i - b_i) \cdot \ln(1 - \theta_i^\Lambda) \right) \quad (6)$$

The first derivative is then

$$\frac{\partial L(\Lambda)}{\partial \Lambda} = \sum_{i=1}^m \left(0 + b_i \cdot e^\Lambda \cdot \ln(\theta_i) - \frac{(n_i - b_i) \cdot e^\Lambda \cdot \theta_i^{e^\Lambda}}{(1 - \theta_i^{e^\Lambda})} \cdot \ln(\theta_i) \right)$$

$\ln(\theta_i)$ can be replaced with $-v_i$:

$$= e^\Lambda \cdot \sum_{i=1}^m \left(-b_i \cdot v_i + \frac{(n_i - b_i) \cdot v_i \cdot \theta_i^{e^\Lambda}}{(1 - \theta_i^{e^\Lambda})} \right)$$

substituting $(n_i - t_i)$ for b_i (where t_i is the number of positive wells)

$$= e^\Lambda \cdot \sum_{i=1}^m \left(-n_i \cdot v_i + t_i \cdot v_i + \frac{t_i \cdot v_i \cdot \theta_i^{e^\Lambda}}{(1 - \theta_i^{e^\Lambda})} \right)$$

rearranging to put all t_i 's over the denominator

$$=e^{\Lambda} \cdot \sum_{i=1}^m \left(-n_i \cdot v_i + \frac{t_i \cdot v_i}{(1-\theta_i^{e^{\Lambda}})} - \frac{t_i \cdot v_i \cdot \theta_i^{e^{\Lambda}}}{(1-\theta_i^{e^{\Lambda}})} + \frac{t_i \cdot v_i \cdot \theta_i^{e^{\Lambda}}}{(1-\theta_i^{e^{\Lambda}})} \right)$$

and simplifying and rearranging in terms of b_i

$$\frac{\partial L(\Lambda)}{\partial \Lambda} = e^{\Lambda} \cdot \sum_{i=1}^m \left(-n_i \cdot v_i + \frac{(n_i - b_i) \cdot v_i}{(1 - \theta_i^{e^{\Lambda}})} \right) \quad (7)$$

Setting Eq. 7 equal to 0, re-substituting λ , and rearranging then gives Eq. 8. By solving Eq. 8 for λ , the expected concentration can be determined from the number of empty wells. This can be done using any solver function, and the accompanying code MVdPCR_MLE.m (see Experimental Section) performs this step using a globalized Newton method.

$$\sum_{i=1}^m n_i \cdot v_i = \sum_{i=1}^m \frac{(n_i - b) \cdot v_i}{(1 - e^{-v_i \cdot \lambda})} \quad (8)$$

The standard error, σ , for a result can be found by using the Fisher information, $I(X)$, for $\ln(\lambda)$,⁴⁴ requiring the change of variable to Λ . The Fisher information is defined in Eq. 9, where $E[\cdot]$ represents the expected value of the given variable.

$$\frac{1}{\text{variance}} = \frac{1}{\sigma^2} = I(\Lambda) = - \int \frac{\partial^2 L(\Lambda)}{\partial \Lambda^2} f(x; \theta) dx = E \left[- \frac{\partial^2 L(\Lambda)}{\partial \Lambda^2} \right] \quad (9)$$

In Eq. 10, the second derivative of Eq. 6 is found.

$$\begin{aligned} \frac{\partial^2 L(\Lambda)}{\partial \Lambda^2} &= e^{\Lambda} \cdot \sum_{i=1}^m \left(-n_i \cdot v_i + \frac{(n_i - b_i) \cdot v_i}{(1 - \theta_i^{e^{\Lambda}})} \right) + e^{\Lambda} \cdot \sum_{i=1}^m \left(\frac{e^{\Lambda} \cdot (n_i - b_i) \cdot \theta_i^{e^{\Lambda} - 1} \cdot v_i \cdot (\ln \theta)}{(1 - \theta_i^{e^{\Lambda}})^2} \right) \\ &= e^{\Lambda} \cdot \sum_{i=1}^m \left(n_i \cdot v_i - \frac{(n_i - b_i) \cdot v_i}{(1 - \theta_i^{e^{\Lambda}})} \right) + (e^{\Lambda})^2 \cdot \sum_{i=1}^m \left(\frac{(n_i - b_i) \cdot v_i^2 \cdot \theta_i^{e^{\Lambda} - 1}}{(1 - \theta_i^{e^{\Lambda}})^2} \right) \end{aligned} \quad (10)$$

Using this expression in Eq. 9 to then find the inverse variance gives Eq. 11

$$\begin{aligned} \frac{1}{\sigma^2} &= -E \left[e^{\Lambda} \cdot \sum_{i=1}^m \left(n_i \cdot v_i - \frac{(n_i - b_i) \cdot v_i}{(1 - \theta_i^{e^{\Lambda}})} \right) + (e^{\Lambda})^2 \cdot \sum_{i=1}^m \left(\frac{(n_i - b_i) \cdot v_i^2 \cdot \theta_i^{e^{\Lambda} - 1}}{(1 - \theta_i^{e^{\Lambda}})^2} \right) \right] \\ &= -e^{\Lambda} \cdot \sum_{i=1}^m \left(n_i \cdot v_i - \frac{(n_i - E[b_i]) \cdot v_i}{(1 - \theta_i^{e^{\Lambda}})} \right) + (e^{\Lambda})^2 \cdot \sum_{i=1}^m \left(\frac{(n_i - E[b_i]) \cdot v_i^2 \cdot \theta_i^{e^{\Lambda} - 1}}{(1 - \theta_i^{e^{\Lambda}})^2} \right) \end{aligned}$$

With $E[b_i]$ coming from Eq. 2

$$\begin{aligned}
&= -e^\Lambda \cdot \sum_{i=1}^m \left(n_i \cdot v_i - \frac{(n_i - n_i \cdot \theta_i^\Lambda) \cdot v_i}{(1 - \theta_i^\Lambda)} \right) + (e^\Lambda)^2 \cdot \sum_{i=1}^m \left(\frac{(n_i - n_i \cdot \theta_i^\Lambda) \cdot v_i^2 \cdot \theta_i^\Lambda}{(1 - \theta_i^\Lambda)^2} \right) \\
&= -e^\Lambda \cdot \sum_{i=1}^m \left(n_i \cdot v_i - n_i \cdot v_i \cdot \frac{(1 - \theta_i^\Lambda)}{(1 - \theta_i^\Lambda)} \right) + (e^\Lambda)^2 \cdot \sum_{i=1}^m \left(\frac{n_i \cdot (1 - \theta_i^\Lambda) \cdot v_i^2 \cdot \theta_i^\Lambda}{(1 - \theta_i^\Lambda)^2} \right) \\
&= (e^\Lambda)^2 \cdot \sum_{i=1}^m \left(\frac{n_i \cdot v_i^2 \cdot \theta_i^\Lambda}{(1 - \theta_i^\Lambda)} \right) = \lambda^2 \cdot \sum_{i=1}^m \left(\frac{n_i \cdot v_i^2 \cdot e^{-v_i \cdot \Lambda}}{(1 - e^{-v_i \cdot \Lambda})} \right) \\
&= \lambda^2 \cdot \sum_{i=1}^m \left(\frac{n_i \cdot v_i^2}{(e^{v_i \cdot \Lambda} - 1)} \right) \tag{11}
\end{aligned}$$

This ultimately gives the standard error (Eq. 12), from which confidence intervals can be generated (Eq. 13), where Z is the upper critical value for the standard normal distribution,

$$\sigma = \frac{1}{\sqrt{\lambda^2 \cdot \sum_{i=1}^m \frac{v_i^2 \cdot n_i}{e^{v_i \cdot \Lambda} - 1}}} \tag{12}$$

$$CI = \ln(\lambda) \pm Z \cdot \sigma \tag{13}$$

One core design requirement of the device is to be able to achieve a certain resolution (that is, distinguish a certain difference in concentration) at certain concentrations. As mentioned above for HIV viral load monitoring, an ideal system would be able to achieve 3-fold resolution for as low as 500 molecules/mL. To be able to correctly resolve two different concentrations, the risk of both false positives (Type I error), and false negatives (Type II error) need to be taken into account.^{6,35,36,39,61} Samples must give results at the desired confidence level (1- α , measure of Type I error), and demonstrate this confidence level again and again (Power: 1- β , measure of Type II error). When comparing two results, the null hypothesis is that the results come from samples that have statistically the same concentration. α is the probability that two results that are determined to be statistically different are in fact from the same sample, thus resulting in a false positive. A 95% confidence level would correspond to $\alpha=0.05$, and an accepted false positive rate of 5%. The power level measures the probability, β , that samples that are statistically different at the desired confidence level give results that fall below this confidence level. A 95% power level would correspond to $\beta=0.05$ and thus an accepted false negative rate of 5%. For the analysis described in this paper, the 3-fold resolution is defined such that samples with a 3-fold difference in concentration (e.g. 500 and 1500 molecules/mL) will give results that are statistically different with at least 95% confidence ($\alpha < 0.05$, less than 5% false positives) at least 95% of the time (power level of 95%, $\beta < 0.05$, no more than 5% false negatives).

The Z-test (Eq. 14) was chosen to measure the confidence level, where λ and σ are calculated using Eq. 8 and 12 respectively for a set of two results (the specific number of negatives, b_i , out of the total number of wells, n_i , at each volume i of wells). The Z-test measures the probability that results are statistically different, by assuming that the test statistics (left side of Eq. 14) can be approximated by a standard normal distribution, so Z corresponds to a known probability. The power level is measured by simulating results from two different samples and determining the probability that they will give results that at least meet the desired confidence level.

$$\frac{\lambda_1 - \lambda_2}{\sqrt{\sigma_1^2 + \sigma_2^2}} = Z, \text{ for 95\% confidence } \frac{\lambda_1 - \lambda_2}{\sqrt{\sigma_1^2 + \sigma_2^2}} > 1.96 \quad (14)$$

For the Z-test, which assumes a normal distribution, to be useful, it is important to verify that it can be used under a wide range of conditions, including at low concentrations when there are few positive wells, or when the design consists of very few wells. While in the limit of many wells the binomial distribution can be approximated by a normal distribution, it is not obvious that a normal approximation is appropriate for the test statistic generated from the MPN-combined binomial distributions. To validate the use of the Z-test under these conditions, the confidence level measured from the Z-test was compared to the confidence level measured based on permutation tests. The permutation test^{62–64} is an exact method for determining the confidence level based on the actual statistical distribution of two results being compared. It was performed here by first determining the concentration that would correspond to the null hypothesis for the two sets of results. The null hypothesis concentration was used to generate simulated sets of results (10,000 simulations), and the confidence level was calculated based on where the original two results fell within the simulated distribution. The results from the Z-test and permutation test are in very good agreement for designs with 160 wells, and even for designs with much fewer wells (Table S1 and as used in the accompanying paper⁵⁵).

Device Design

To meet the design requirements to monitor HIV viral load, a multivolume device was designed with 160 wells each at volumes of 125, 25, 5 and 1 nL (Table 1). A radial layout of wells (Figure 2) provides an efficient use of space when wells of significantly different volumes are used. In the initial orientation of the radial multivolume SlipChip, the main wells are aligned to create a continuous fluidic path that allows all of the sample wells to be filled in one step using dead end filling.⁵² The SlipChip can then be rotationally slipped (~ 8°) to simultaneously isolate each well and overlap it with the corresponding thermal expansion well (Figure 2). This device has a LDL of 120 molecules/mL and a dynamic range where at least 3-fold resolution is achieved from 520 – 3,980,000 molecules/mL (Table 1).

To validate both the statistical analysis and the performance of the device, experiments were carried out to test the theoretical predictions. Many experiments were required to obtain sufficient statistics, and nine SlipChips were used for experiments. To minimize variability among experiments, the etching depth of the chips was closely monitored during the fabrication process. Due to the variations in the printed masks and the actual etch depths during fabrication, the actual volumes of the nominal 125, 25 5 and 1 nL wells were, on average, 127.47, 27.51, 5.03 and 1.12 nL respectively, with a coefficient of variation between chips of 0.2–0.5% for the average well size and 0.7–1.1% for individual wells (see details in Supporting Information, Table S2). Due to the small variation between chips, the average volumes were used for analysis to calculate the sample concentrations.

Experimental Validation

A control 631 bp sequence of DNA was used to validate the MV digital PCR approach. A stock solution of DNA of well-defined sequence and length was generated by using PCR with subsequent purification (See Experimental Section and sequence and primers in Supporting Information). The initial concentration of this stock solution was determined by UV-Vis, and the stock was then diluted to levels required for testing of the chip. Concentrations were tested across the entire dynamic range of the device: approximately

500, 1500, 8000, 20,000, 30,000, 100,000, 600,000 and 3,000,000 molecules/mL. A total of 80 experiments and 29 additional controls were performed, and the observed concentrations showed excellent agreement with the expected concentrations and demonstrated the accuracy of the device performance over the entire dynamic range (Figure 3). The experimental results consist of a “digital” pattern of positive and negative wells. At a low input concentration of 1500 molecules/mL (Figure 3a), the larger 125 and 25 nL wells provide the majority of the information to determine the concentration. As expected, at a higher concentration of 600,000 molecules/mL, positives were found in the smaller 5 and 1 nL wells also (Figure 3b), and these smaller wells provide the majority of the information used to determine the concentration. Excellent agreement was found between the input concentration and the measured concentration over four orders of magnitude (Figure 3c, d). These experiments were performed over a period spanning over four months independently by two of the authors using multiple aliquots of DNA. Of the 80 results, 65 fell within the 95% CI and 76 of the 80 results fell within the 99% CI. Experimental error (including potential for DNA degradation over time and dilution and pipetting errors) has likely made a contribution to the minor broadening of the distribution of results beyond those statistically predicted, but we consider the overall agreement to be quite good (Figure 3d). In this multivolume design the 95% confidence interval is narrow at a consistent level over a very large range of concentrations: the CI is within 13.8–15% of the expected value from 9500–680,000 molecules/mL and within 13.8–17.5% from 5400–1,700,000 molecules/mL. The experimental data tracked closely the theoretically predicted CI (Figure 3d).

As expected the largest wells (125 nL) provided the largest contribution to the overall confidence interval for samples in the $10^2 - 10^4$ molecules/mL range while the use of smaller and smaller wells down to 1 nL in volume extended the dynamic range with 95% confidence interval above 10^6 molecules/mL (Figure 3c, d). For each concentration there was excellent agreement among the individual results obtained from the wells of different volumes, consistent with the accuracy of the overall device. This agreement is illustrated for an input concentration of 30,000 molecules/mL (Figure 4). At this concentration the wells of all volumes provided a reasonable number of positives and negatives for quantification, and we found that the concentration calculated from the results fell within the 95% confidence intervals for individual volumes of wells (38 of 40 results), and also the averages from wells of each volumes were internally consistent (Figure 4).

Having confirmed that the device performs accurately and precisely, we tested whether the predicted levels of resolution could be achieved. Three-fold resolution was predicted to be attained from a lower limit of quantification (LLQ-3) of 500 molecules/mL, so 20 sets of MV digital PCR experiments were performed using pairs of samples at concentrations of 500 and 1500 molecules/mL. In these experiments, performed by the same author, 19 out of 20 pairs of results fell within >95% confidence range (Table S3), consistent with the expected power level. Pairing the experiments reduces variability due to differences in sample degradation and pipetting errors by different users. Upon randomization of all 20 pairs in Table S3 to produce 1000 pairs of results, the power level was still 92%, indicating that while there is possibly some day-to-day and user-to-user variability, it is not dominating the results. The maximum expected resolution of this chip is about 1.5-fold, and this resolution was tested with pairs of samples at concentrations of 20,000 and 30,000 molecules/mL by two of the authors. Here, 10 sets of experiments were performed, and all 10 pairs showed >95% confidence (Table 2 and Supporting Information, Table S4). For 1.5-fold resolution, even upon randomization of the original 10 pairs in Table 2 and Table S4 (Supporting Information) into 100 sets to produce 1000 pairs of results, a 96.6% power level was maintained.

Protocol to design devices and accompanying computer programs

We provided a protocol for designing devices that combines simple empirical observations with advanced and precise software programs to efficiently design customized systems. Multiple variables influence the overall performance characteristics of MV digital PCR systems including: number of well sizes, number of wells at each volume, and the “volumetric step”, VS, (the multiplication factor by which volumes are increased from smallest to largest; VS = 5 was used in this paper). The first step in device design is to identify the requirements for performance of the device and any physical limitations on the design. Physical limitations include limits on fabrication (volumes of smallest or largest wells, or specific dimensions such as depth and/or cross section), and constraints on the overall size of the device as a function of the number of wells used. We describe the performance of each design in terms of parameters LDL, LLQ-X, ULQ-X, and ULQ, which are defined and described below.

The lower detection limit, LDL, is defined as the concentration which would have a 95% probability of generating a least one positive well, i.e. a 95% probability of having at least one molecule in the total volume of all wells. The actual concentration is then set by the total volume. Applying these conditions to Eq. 1 reveals that this corresponds to an average concentration, λ , of three molecules in the total volume. For the design characterized in this paper, three molecules in 24.96 μL correspond to an average concentration of 120 molecules/mL. This parameter is important to consider when absolute sensitivity is important.

The upper limit of quantification (ULQ) is defined in a similar fashion. Specifically it is the concentration where the probability of all wells being positive is 5%, or in other words there is 95% probability that at least 1 well is negative. The ULQ is a function of both the smallest well volume and the number of wells at that volume. The conditions needed to set the ULQ are determined using Eq. 15, where n and v should be the values for the smallest volume.

$$0.05 = (1 - e^{-(v \cdot \lambda)})^n \quad (15)$$

For the design tested in this paper 1,000,000 molecules/mL was the target for the ULQ, but the device was designed to exceed this to allow for potential increases in concentration during sample preparation. Setting $\lambda=4,000,000$ molecules/mL and testing extreme cases of total number of wells ($n=20$ and 1000) reveals that the smallest volume will be in the range of 0.5–1.5 nL. The actual size and number of the smallest volume wells can then be determined by preferences of fabrication. For example, if 1 nL is the smallest volume that can be easily fabricated and utilized, then to detect $\lambda=4,000,000$ molecules/mL, about 160 wells are needed at this volume. Setting the ULQ is a critical factor when setting the dynamic range and the number of wells used in the design.

The lowest concentration that the design can distinguish statistically from a concentration X-fold higher with the desired confidence and power limits is defined as the lower limit of quantification for X-fold resolution (LLQ-X). Similarly the highest concentration at which X-fold resolution can be achieved is designated ULQ-X. Depending on the resolution level, the ULQ defined above can also coincide with the ULQ-X. Resolving concentrations is a critical aspect of the design for quantification. For the LLQ-X, a minimum number of positive wells is required. This minimum number is dependent on the total number of wells, and decreases to an asymptotic limit as the total number of wells increases, (summarized in Table 3 and Figure 5 for a single volume system with requirements of 95% confidence and 95% power criteria used in this paper). For 3-fold resolution, 13 positives are needed and 13

molecules/(500 molecules/mL) = 26 μ L, thus setting an approximate bound on the total volume of all wells.

Barring special circumstances, it is simplest for design and analysis to have the same number of wells at each volume and to have the volumes related by the same VS. More wells result in better resolution, but more total space would be required. A smaller VS results in more overlap between volumes and thus better resolution, but decreases the size of the dynamic range; a larger VS has the opposite effect. The above methods provide simple starting points to design systems, but several designs can meet the desired parameters. More precise analysis is required to ensure that the target design criteria are met and that the chosen design is near-optimal. The performance of each potential system can be tested via simulations to select the most suitable design. To enable more quantitative design of MV digital PCR devices, a series of computer programs were written. These programs are provided in the SI, along with their descriptions in the “Computer Programs” section. These programs were used to analyze several designs to illustrate the general trends that one should keep in mind during the design of MV digital PCR systems (Table 4, Figures 6 and 7, and Supporting Information, Table S5).

First, we quantified how the VS affects resolution and dynamic range for multivolume designs with the same total number of wells and similar total volumes (Table 4 and Figure 6, comparison of four theoretical MV designs and an analogous single-volume design). Under these constraints, the larger the VS, the larger the dynamic range (up to 5.4 orders of magnitude for VS=10), and the lower the achievable resolution. The VS=5 we chose for the device described in this paper provided a suitable balance of resolution (down to 1.5-fold from 10,120–200,000 molecules/mL, 1.3 order of magnitude; 3-fold resolution from 520–3,980,000 molecules/mL, 3.9 order of magnitude) and a dynamic range spanning 4.5 orders of magnitude.

Second, we quantified how VS affects resolution and the required number of wells when we constrain the dynamic range and total volume for each design, and adjust the number of wells at each VS (see Figure 7 and Table S5, comparison of four theoretical MV designs and a single volume design). Under these constraints, multivolume designs required very few wells. For example for a design with VS=10, only 144 total wells were required to achieve 3-fold resolution from 730–1,167,000 molecules/mL, while a single-volume design required 12,000 wells to achieve 3-fold resolution over a range from 495–3,987,000 molecules/mL. The same design with VS =10 and with 144 wells provided 5-fold resolution from 210–3,980,000 molecules/mL, similar to the single-volume design with 12,000 wells (180–3,990,000 molecules/mL). The advantage of reducing VS, down to VS = 1 for the single-volume design, is in providing higher resolution (13,500–3,990,000 molecules/mL at 1.3-fold and down to 1.1-fold from 127,000–2,250,000 molecules/mL) that cannot be provided by multivolume designs unless they also contain many wells. When resolution needs to be maximized, single volume systems with many wells have a clear advantage as evidenced by the application of such systems for prenatal aneuploidy detection^{30,37,41} and detection of copy number variations and genetic mutations related to cancer and other diseases.^{16,27,30,33,35,38,40} Finally, for the device that we validated experimentally in this paper (Design 3 in Tables 4 and Supporting Information Table S5), we plotted the range of concentrations over which different levels of resolution are maintained (Figure 8) using MVdPCR_RunPlot.m. As expected, 5-, 3-, and 2- fold resolution was maintained over a large portion of the dynamic range, with the limit for this device of ~ 1.5-fold resolution at 95% power with at least 95% confidence. For this device the number of wells and VS used leads to a significant overlap of confidence intervals for sets of wells of different volumes, and therefore the combined CI is smooth over the much of the dynamic range (also CI curves of Figure 3c and d). If VS is too large and small numbers of wells are used, or if only

single volumes are used (see individual CI curves of Figure 3c and d), the combined CI curve may follow the variation of the CIs for individual volumes, which would be undesirable (Figure 8b).

Conclusions

In this paper, we described an approach to improve “digital” (single molecule) assays and validated it using digital PCR amplification. This platform, MV digital PCR, uses wells at multiple volumes to quantify nucleic acids at high dynamic range and high resolution while minimizing the total number of wells. By using different well volumes, the upper and lower limits of quantification are effectively decoupled to achieve the desired performance specifications. By reducing the total number of wells, a MV system allows for simpler device design, minimizes sample handling, reduces contamination risks, allows for multiplexing by allowing for multiple assays to be performed on a single chip, and reduces the use of reagent when compared to the multiple sample dilutions required by serial dilution.

We tested predictions of the theory by creating a rotational SlipChip designed to satisfy requirements for quantifying HIV viral load. For this chip, we have shown experimental agreement with mathematical theory over the entire dynamic range, accurate absolute quantification, and agreement between predicted and experimentally observed resolution. Results from different volumes enabled more precise and accurate results than would be obtained from any single volume. Separately analyzing the experimental results from different sets of well volumes provided a direct source for internal controls, and we demonstrated that, at least when using purified DNA and this specific PCR chemistry implemented on SlipChip, there were no artifacts due to different surface-to-volume ratios or variable concentrations of single molecules in wells of different volumes. This result would have to be confirmed further when other chemistries or more complex sample matrixes⁵⁵ are used.

In cases when the distribution of concentrations in samples is bimodal, i.e. when some samples require quantification at high concentrations and others at low concentrations, multivolume systems with non-uniform volumetric steps could be used. A multiplexed multivolume system with identical dynamic range and resolution for each sample is described in the accompanying paper,⁵⁵ but multiplexed systems can also be designed where different regions of the device can probe different dynamic ranges and/or different resolutions by varying the volumes of individual wells and the number of wells at each volume.

By integrating isothermal amplification and reverse-transcription methods, visual readout, and sample preparation with the MV digital PCR SlipChip, this approach would be more widely applicable to quantification of nucleic acids under resource-limited settings. The multivolume approach simplifies readout and analysis because there are fewer wells to visualize and analyze. SlipChip devices are compatible with other amplification chemistries beyond PCR, such as recombinase polymerase amplification,⁵⁶ and we expect that digital isothermal chemistries will be successfully used in multivolume devices, although it remains to be experimentally confirmed. Reverse-transcription to quantify HIV and HCV viral RNA in multivolume devices is described in the accompanying paper.⁵⁵ The MV digital approach described here is also applicable in other fields that depend on Poisson statistics for interpretation, including digital immunoassays^{65,66} and stochastic confinement of bacteria^{67,68} or other cells.

We emphasize that the presented design guidelines and software programs are not limited to multivolume devices, and even current single-volume digital PCR methods would benefit from these facile in-depth design and analysis tools.²⁶ Single-volume devices that use dilution series are mathematically equivalent to multivolume devices, and the approach presented here can be applied to design and analysis of dilution series. Finally, the theory and software developed here is not limited to SlipChip, and is also applicable to design and analysis of other digital analysis systems,^{24,26,28,30,65,66} including valve-based^{25,27,34,41} or droplet-based systems.^{29,32,36,69,70}

Supplementary Material

Refer to Web version on PubMed Central for supplementary material.

Acknowledgments

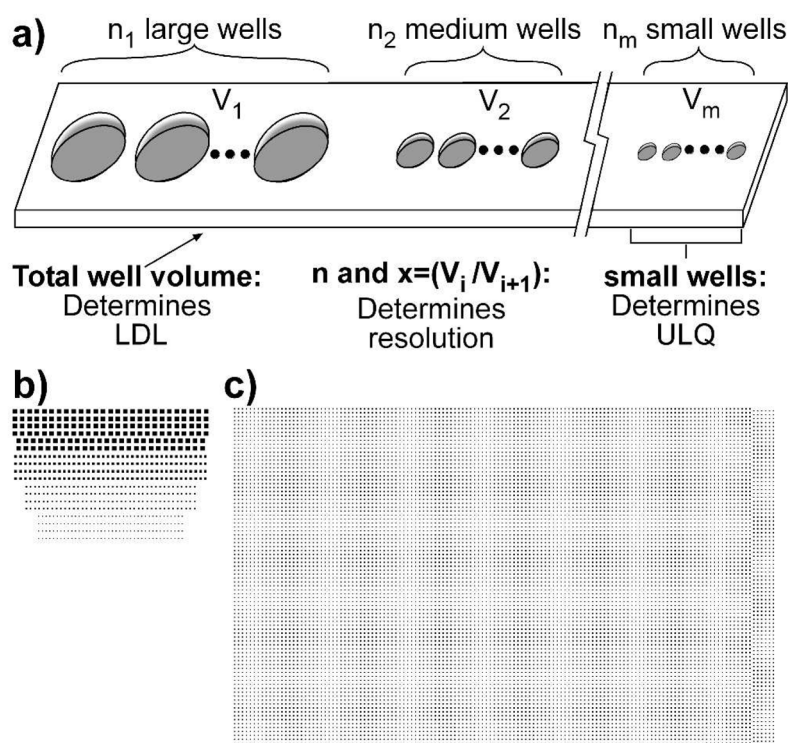
This work was supported by the NIH Director's Pioneer Award program, part of the NIH Roadmap for Medical Research (1 DP1 OD003584) and NIH Grant No. 1R01 EB012946 administered by the National Institute of Biomedical Imaging and Bioengineering and the Office of Advanced Scientific Computing Research, Office of Science, U.S. Department of Energy, under Contract DE-AC02-06CH11357. We thank Mary-Sara McPeck, Margaret Loudermilk, and Ian Foster for helpful discussion of the statistical analysis.

References

1. Brambilla D, Reichelderfer PS, Bremer JW, Shapiro DE, Hershov RC, Katzenstein DA, Hammer SM, Jackson B, Collier AC, Sperling RS, Fowler MG, Coombs RW. *AIDS*. 1999; 13:2269–2279. [PubMed: 10563712]
2. Calmy A, Ford N, Hirschel B, Reynolds SJ, Lynen L, Goemaere E, de la Vega FG, Perrin L, Rodriguez W. *Clin Infect Dis*. 2007; 44:128–134. [PubMed: 17143828]
3. Ginocchio CC, Kemper M, Stellrecht KA, Witt DJ. *J Clin Microbiol*. 2003; 41:164–173. [PubMed: 12517843]
4. Keiser O, et al. *AIDS*. 2009; 23:1867–1874. [PubMed: 19531928]
5. Scott LE, Noble LD, Moloi J, Erasmus L, Venter WDF, Stevens W. *J Clin Microbiol*. 2009; 47:2209–2217. [PubMed: 19420172]
6. Urdea M, Penny LA, Olmsted SS, Giovanni MY, Kaspar P, Shepherd A, Wilson P, Dahl CA, Buchsbaum S, Moeller G, Hay Burgess DC. 2006; 444(Suppl 1):73–79.
7. Wang SQ, Xu F, Demirci U. *Biotechnol Adv*. 2010; 28:770–781. [PubMed: 20600784]
8. Yen MH, Tsao KC, Huang YC, Huang CG, Huang YL, Lin RY, Chang ML, Huang CC, Yan DC, Lin TY. *Clin Infect Dis*. 2007; 44:E78–E81. [PubMed: 17443457]
9. Niesters HGM. *Methods*. 2001; 25:419–429. [PubMed: 11846611]
10. Humar A, Paya C, Pescovitz MD, Dominguez E, Washburn K, Blumberg E, Alexander B, Freeman R, Heaton N, Mueller B. *Am J Transplant*. 2004; 4:644–649. [PubMed: 15023158]
11. Landry ML, Garner R, Ferguson D. *J Clin Microbiol*. 2005; 43:3136–3139. [PubMed: 16000425]
12. Gersberg RM, Rose MA, Robles-Sikisaka R, Dhar AK. *Appl Environ Microbiol*. 2006; 72:7438–7444. [PubMed: 16980430]
13. Carey CM, Lee H, Trevors JT. *J Microbiol Methods*. 2006; 67:363–372. [PubMed: 16730821]
14. Fredslund L, Ekelund F, Jacobsen CS, Johnsen K. *Appl Environ Microbiol*. 2001; 67:1613–1618. [PubMed: 11282613]
15. Martin B, Jofre A, Garriga M, Hugas M, Aymerich T. *Lett Appl Microbiol*. 2004; 39:290–295. [PubMed: 15287877]
16. Goh HG, Lin M, Fukushima T, Saglio G, Kim D, Choi SY, Kim SH, Lee J, Lee YS, Oh SM, Kim DW. *Leuk Lymphoma*. 2011; 52:896–904. [PubMed: 21338281]
17. Kern W, Schoch C, Haferlach T, Schnittger S. *Crit Rev Oncol/Hematol*. 2005; 56:283–309.

18. Chen CF, Ridzon DA, Broomer AJ, Zhou ZH, Lee DH, Nguyen JT, Barbisin M, Xu NL, Mahuvakar VR, Andersen MR, Lao KQ, Livak KJ, Guegler KJ. *Nucleic Acids Res.* 2005; 33:e179. [PubMed: 16314309]
19. Espy MJ, Uhl JR, Sloan LM, Buckwalter SP, Jones MF, Vetter EA, Yao JDC, Wengenack NL, Rosenblatt JE, Cockerill FR, Smith TF. *Clin Microbiol Rev.* 2006; 19:165–256. [PubMed: 16418529]
20. Murphy J, Bustin SA. *Expert Rev Mol Diagn.* 2009; 9:187–197. [PubMed: 19298142]
21. Bustin SA, Benes V, Nolan T, Pfaffl MW. *J Mol Endocrinol.* 2005; 34:597–601. [PubMed: 15956331]
22. Huggett J, Dheda K, Bustin S, Zumla A. *Genes Immun.* 2005; 6:279–284. [PubMed: 15815687]
23. Burns MJ, Burrell AM, Foy CA. *Eur Food Res Technol.* 2010; 231:353–362.
24. Vogelstein B, Kinzler KW. *Proc Natl Acad Sci USA.* 1999; 96:9236–9241. [PubMed: 10430926]
25. Ottesen EA, Hong JW, Quake SR, Leadbetter JR. *Science.* 2006; 314:1464–1467. [PubMed: 17138901]
26. Applied Biosystems, Life Technologies. Digital PCR Using the OpenArray® Real Time PCR System. 2010.
<http://www.appliedbiosystems.com/absite/us/en/home/applications-technologies/real-time-pcr/real-time-pcr-instruments/openarray-real-time-pcr-system/digital-pcr-using-openarray.html>
27. Dube S, Qin J, Ramakrishnan R. *PLoS One.* 2008; 3
28. Sundberg SO, Wittwer CT, Gao C, Gale BK. *Anal Chem.* 2010; 82:1546–1550. [PubMed: 20085301]
29. Zeng Y, Novak R, Shuga J, Smith MT, Mathies RA. *Anal Chem.* 2010; 82:3183–3190. [PubMed: 20192178]
30. Zhang C, Da X. *Chem Rev.* 2010; 110:4910–4947. [PubMed: 20394378]
31. Shen F, Du WB, Kreutz JE, Fok A, Ismagilov RF. *Lab Chip.* 2010; 10:2666–2672. [PubMed: 20596567]
32. Kiss MM, Ortoleva-Donnelly L, Beer NR, Warner J, Bailey CG, Colston BW, Rothberg JM, Link DR, Leamon JH. *Anal Chem.* 2008; 80:8975–8981. [PubMed: 19551929]
33. Bhat S, Herrmann J, Armishaw P, Corbisier P, Emslie KR. *Anal Bioanal Chem.* 2009; 394:457–467. [PubMed: 19288230]
34. Warren L, Bryder D, Weissman IL, Quake SR. *Proc Natl Acad Sci U S A.* 2006; 103:17807–17812. [PubMed: 17098862]
35. Weaver S, Dube S, Mir A, Qin J, Sun G, Ramakrishnan R, Jones RC, Livak KJ. *Methods.* 2010; 50:271–276. [PubMed: 20079846]
36. Li M, et al. *Nat Biotechnol.* 2009; 27:858–863. [PubMed: 19684580]
37. Lo YMD, Lun FMF, Chan KCA, Tsui NBY, Chong KC, Lau TK, Leung TY, Zee BCY, Cantor CR, Chiu RWK. *Proc Natl Acad Sci U S A.* 2007; 104:13116–13121. [PubMed: 17664418]
38. El Karoui N, Zhou W, Whittemore AS. *Stat Med.* 2006; 25:3124–3133. [PubMed: 16397858]
39. Chu TJ, Bunce K, Hogge WA, Peters DG. *Bioinformatics.* 2010; 26:2863–2866. [PubMed: 20870643]
40. Diehl F, Diaz LA. *Curr Opin Oncol.* 2007; 19:36–42. [PubMed: 17133110]
41. Fan HC, Quake SR. *Anal Chem.* 2007; 79:7576–7579. [PubMed: 17715994]
42. Cochran WG. *Biometrics.* 1950; 6:105–116. [PubMed: 15420239]
43. Destgroth SF. *J Immunol Methods.* 1982; 49:R11–R23. [PubMed: 7040548]
44. Hurley MA, Roscoe ME. *J Appl Bacteriol.* 1983; 55:159–164.
45. Halvorson HO, Ziegler NR. *J Bacteriol.* 1933; 25:101–121. [PubMed: 16559606]
46. Halvorson HO, Ziegler NR. *J Bacteriol.* 1933; 26:559–567. [PubMed: 16559678]
47. Kinzelman JL, Singh A, Ng C, Pond KR, Bagley RC, Gradus S. *Lake Reserv Manag.* 2005; 21:73–77.
48. Kodaka H, Saito M, Matsuoka H. *Biocontrol Sci.* 2009; 14:123–126. [PubMed: 19785286]
49. Sercu B, Van De Werfhorst LC, Murray JLS, Holden PA. *Appl Environ Microbiol.* 2011; 77:627–633. [PubMed: 21097584]

50. Du WB, Li L, Nichols KP, Ismagilov RF. *Lab Chip*. 2009; 9:2286–2292. [PubMed: 19636458]
51. Li L, Du WB, Ismagilov RF. *J Am Chem Soc*. 2010; 132:106–111. [PubMed: 20000708]
52. Li L, Karymov MA, Nichols KP, Ismagilov RF. *Langmuir*. 2010; 26:12465–12471. [PubMed: 20575548]
53. Liu WS, Chen DL, Du WB, Nichols KP, Ismagilov RF. *Anal Chem*. 2010; 82:3276–3282. [PubMed: 20334360]
54. Shen F, Du WB, Davydova EK, Karymov MA, Pandey J, Ismagilov RF. *Anal Chem*. 2010; 82:4606–4612. [PubMed: 20446698]
55. Shen F, Sun B, Kreutz JE, Davydova EK, Du WB, Reddy P, Joseph L, Ismagilov RF. *J Am Chem Soc*. 2011 submitted.
56. Shen F, Davydova EK, Du WB, Kreutz JE, Piepenburg O, Ismagilov RF. *Anal Chem*. 2011; 83:3533–3540. [PubMed: 21476587]
57. Blainey PC, Quake SR. *Nucleic Acids Res*. 2011; 39
58. Mazutis L, Araghi AF, Miller OJ, Baret JC, Frenz L, Janoshazi A, Taly V, Miller BJ, Hutchison JB, Link D, Griffiths AD, Ryckelynck M. *Anal Chem*. 2009; 81:4813–4821. [PubMed: 19518143]
59. Agresti A, Coull BA. *Am Stat*. 1998; 52:119–126.
60. Wilson EB. *J Am Stat Assoc*. 1927; 22:209–212.
61. Lieber RL. *J Orthop Res*. 1990; 8:304–309. [PubMed: 2303964]
62. Oden A, Wedel H. *Ann Stat*. 1975; 3:518–520.
63. Welch WJ. *J Am Stat Assoc*. 1990; 85:693–698.
64. Pitman EJC. *Biometrika*. 1938; 29:322–335.
65. Rissin DM, Kan CW, Campbell TG, Howes SC, Fournier DR, Song L, Piech T, Patel PP, Chang L, Rivnak AJ, Ferrell EP, Randall JD, Provuncher GK, Walt DR, Duffy DC. *Nat Biotechnol*. 2010; 28:595–599. [PubMed: 20495550]
66. Rissin DM, Walt DR. *J Am Chem Soc*. 2006; 128:6286–6287. [PubMed: 16683771]
67. Boedicker JQ, Li L, Kline TR, Ismagilov RF. *Lab Chip*. 2008; 8:1265–1272. [PubMed: 18651067]
68. Vincent ME, Liu WS, Haney EB, Ismagilov RF. *Chem Soc Rev*. 2010; 39:974–984. [PubMed: 20179819]
69. Pompano RR, Liu WS, Du WB, Ismagilov RF. *Annual Review of Analytical Chemistry*. *Annual Reviews*. 2011; 4:59–81.
70. Song H, Chen DL, Ismagilov RF. *Angew Chem-Int Edit*. 2006; 45:7336–7356.

**Figure 1.**

a) General schematic of multivolume system used for digital PCR (MV digital PCR), with relationship between device features and performance abilities. Two hypothetical devices with identical dynamic range and with equal spacing ($300\ \mu\text{m}$) between wells: b) a model MV digital PCR system (160 wells each at 125, 25, 5 and 1 nL) and c) a single volume digital PCR system (12,000 wells at 2.08 nL). With these design parameters the footprint of the MV wells is approximately 7 fold smaller than the single volume design. Note: Well sizes are based on assumption of cubic dimensions, and in the MV design the vertical spacing was kept constant from center of well to center of well, as would be required for proper slipping in a SlipChip platform, and is based on a $300\ \mu\text{m}$ spacing between the largest wells.

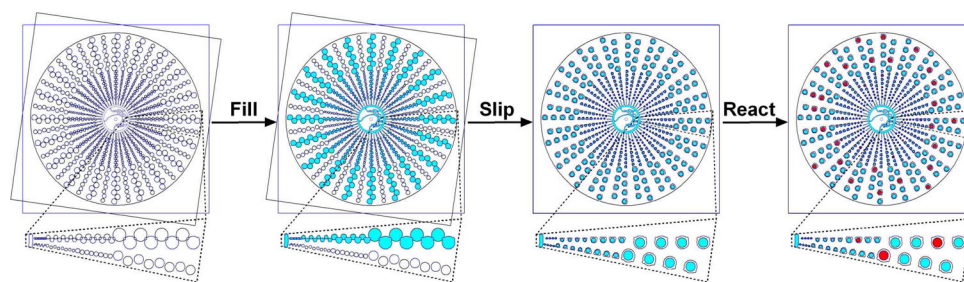


Figure 2. Schematic for radial SlipChip to perform MV digital PCR. Design consists of 160 wells each at 125, 25, 5, and 1 nL. Sample is loaded from the center and after filling is rotationally slipped to isolate wells. After the reaction, wells containing template have enhanced signal and can be counted.

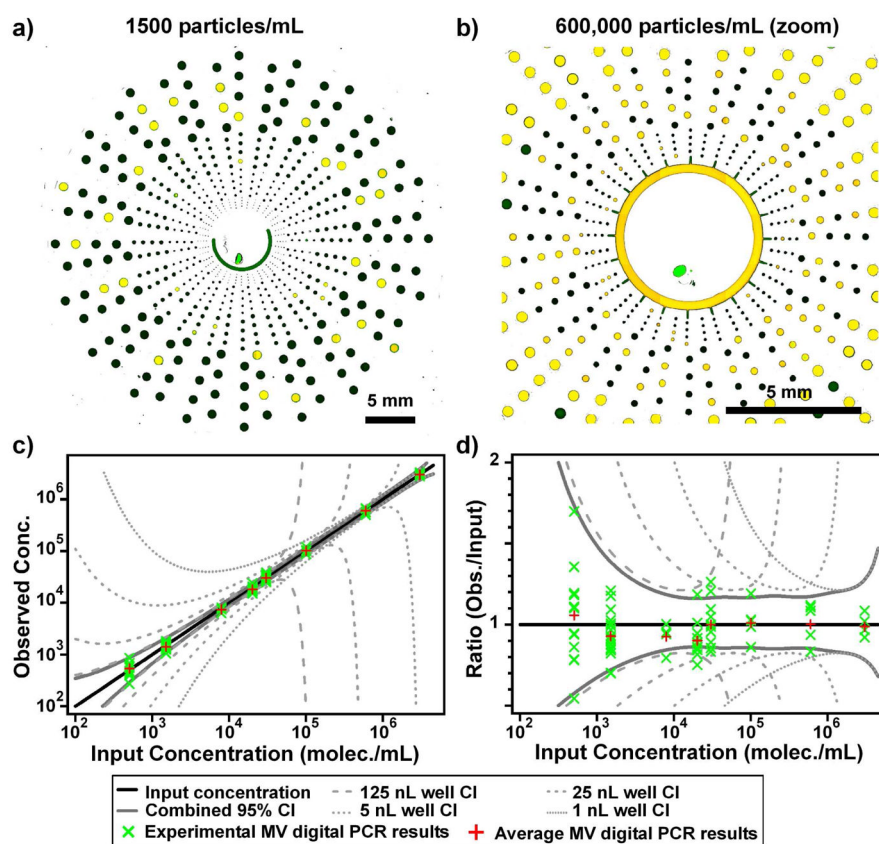


Figure 3.

Experimental results for MV digital PCR on SlipChip using control DNA. Representative false color images (yellow represents positive wells that showed at least a 3-fold increase in intensity compared to negative wells) for solutions with input concentrations of (a) 1500 molecules/mL and (b) 600,000 molecules/mL (zoomed in on smaller wells). c, d Graphical summary of all experiments comparing the input concentration, based on UV-V is measurements (black curve), and observed concentrations using MV digital PCR (× and +) over the entire dynamic range. Represented as (c) the actual concentration and (d) as a ratio to better show distribution of results. Stock samples were approximately 500, 1500, 8000, 20,000, 30,000, 100,000, 600,000 and 3,000,000 molecules/mL. The confidence intervals (CI) for the combined system (solid gray curves) indicate where 95% of the experiments should fall. CI curves for the individual volumes (various dashed gray curves), are also provided to indicate over what range of concentration each volume contributes.

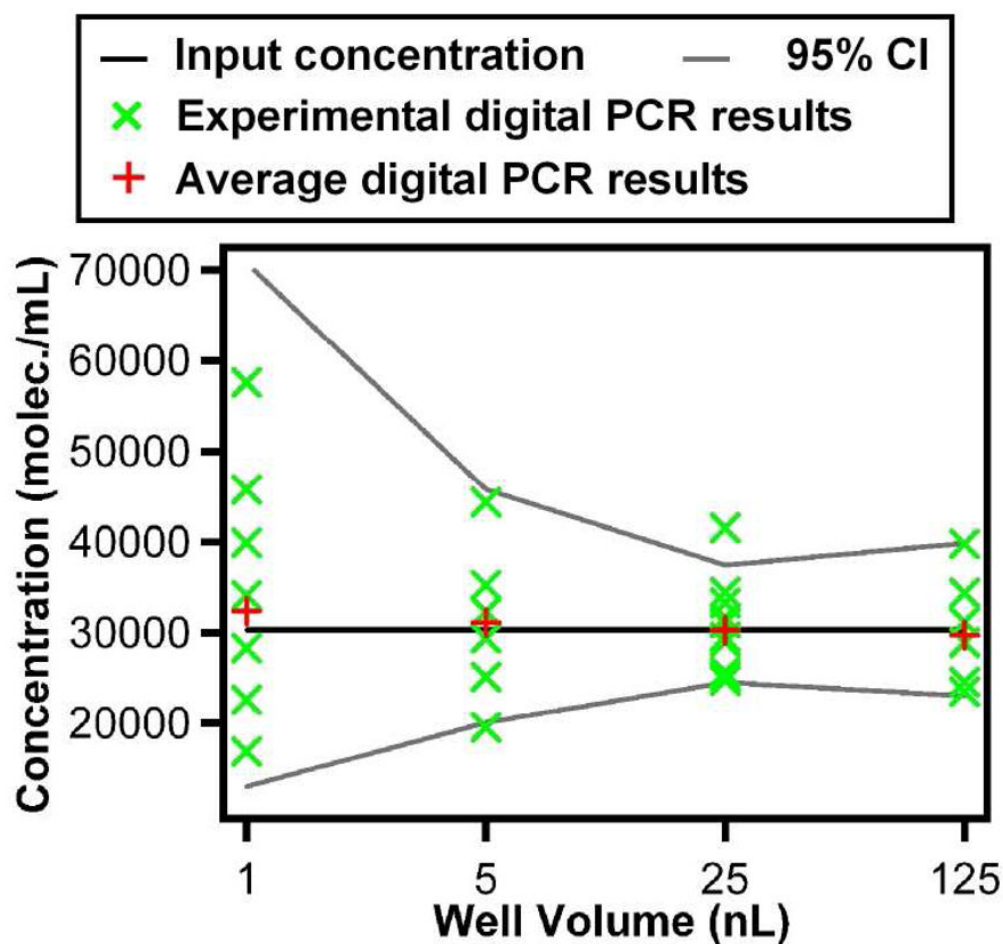


Figure 4. Separate analysis of 10 experimental results for different well volumes with input concentration of 30,000 molecules/mL shows the distribution of measured concentrations for each volume and overall agreement of results.

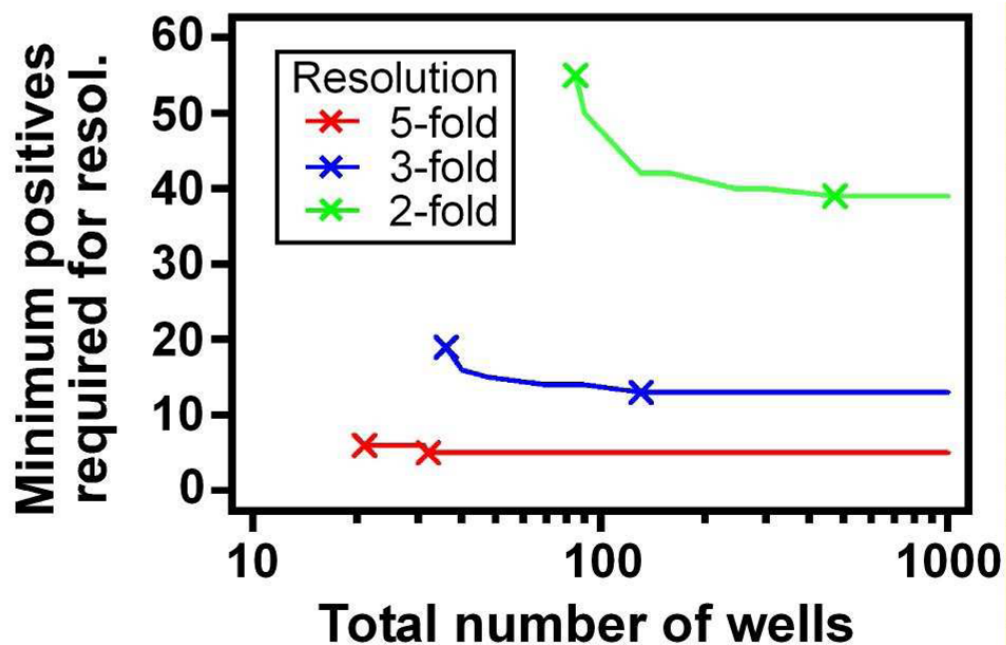


Figure 5. Relationship between the total number of wells in a single-volume system, and the minimum number of positive results required to meet the desired resolution at the LLQ-X. The symbols × correspond to the points listed in Table 3. The ULQ-X limit, not given here but identified in Table 3, is set by the ULQ definition above of having an average concentration corresponding to 3 negative wells in the total volume.

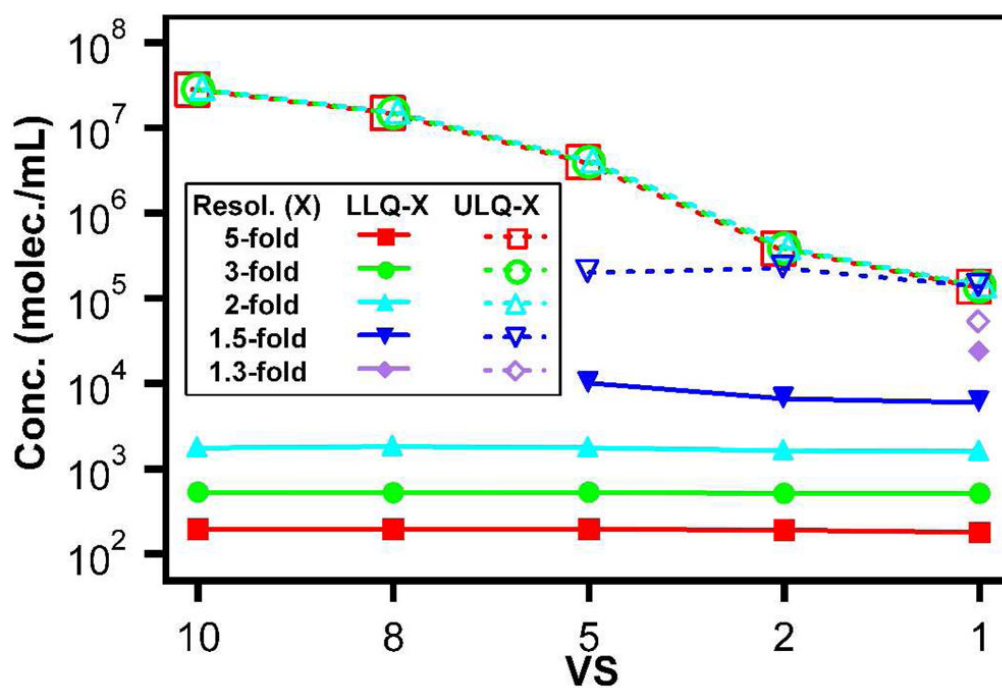


Figure 6. Plot of LLQ-X and ULQ-X as a function of VS at constant total well number and total volume. For each resolution level (X), the minimum (LLQ-X) and maximum (ULQ-X) concentrations that can achieve the desired power level (95%) are given for each design in Table 4. No concentration could be plotted if the resolution level (X) could not be achieved for a given VS.

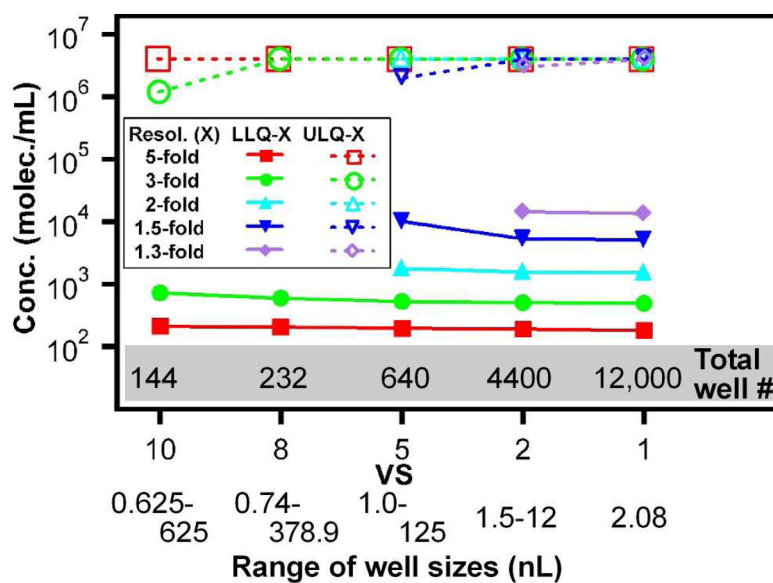


Figure 7.

Plot of LLQ-X and ULQ-X for the designs in Table S5 demonstrates impact of VS on resolution and total number of wells at constant total well number and dynamic range. For VS=10 the design consists of 36 wells each at 625, 62.5, 6.25 and 0.625 nL, for VS=8 the design consists of 58 wells each at 378.9, 47.36, 5.92 and 0.74 nL, for VS=5 the design consists of 160 wells each at 125, 25, 5 and 1 nL, for VS=2 the design consists of 1100 wells each at 12, 6, 3 and 1.5 nL and for VS=1 the design consists of 12,000 wells at 2.08 nL. For all designs the LDL is approximately 120 molecules/mL and the ULQ is approximately 4 million molecules/mL.

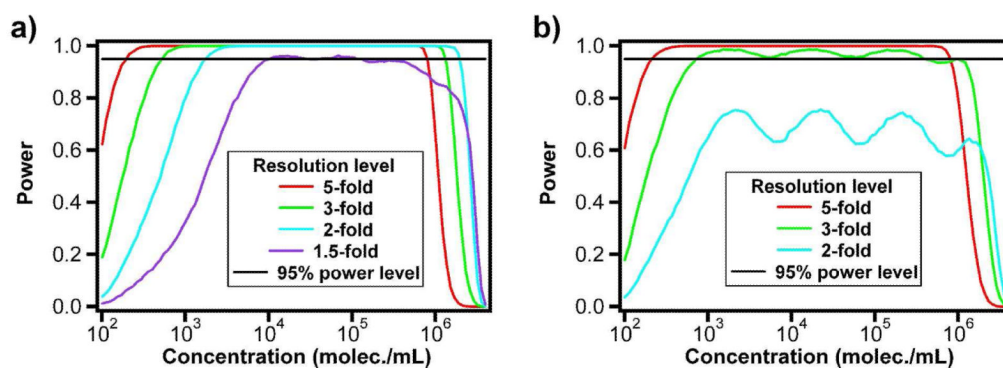


Figure 8.

Simulation results of plots generated from MVdPCR_RunPlot.m for (a) the design used in this paper, and (b) Design 1 from Table S5 (36 wells each at 625, 62.5, 6.25 and 0.625 nL), revealing approximate concentration ranges over which the desired resolution levels are achieved. The curves are for the lower of the two concentrations being resolved. LLQ-X corresponds to the concentration at which the curve rises above 0.95 (black line), and the ULQ-X corresponds to the concentration X times higher than the concentration at which the curve drops back below 0.95.

Table 1

Summary of Device Design, Specifications and Performance

Number of wells	volume per well (nL)	Total volume (µL)	LDL (molec./mL)*	LLQ-5 (molec./mL)**	LLQ-3 (molec./mL)**	ULQ (molec./mL)***
160	125	20	150	250	680	31,800
160	25	4	760	1270	3390	159,000
160	5	0.8	3800	6350	16,950	795,000
160	1	0.16	18,900	31,750	84,700	3,977,000
Overall device (wells of all volumes)		24.96	120	200	520	3,977,000

* LDL is the lower detection limit and is defined as the concentration which would have a 95% chance of generating a least one positive well, and equals the concentration calculated from three positive wells.

** LLQ-5 and LLQ-3 refer to the lower limit of quantification for 5-fold and 3-fold resolution respectively. They correspond to the concentration calculated based on 5 positive wells (for 5-fold resolution) or 13 positive wells (3-fold resolution).

*** ULQ is the upper limit of quantification, and is defined as the concentration which would have a 95% chance of generating at least one negative well, and equals the concentration calculated based on three negative wells. ULQ is reported as the upper of the two concentrations being resolved. For this design ULQ coincides for both 3- or 5-fold resolution.

Table 2

Experimental results testing 1.5-fold resolution (20,000 molecules/mL vs. 30,000 molecules/mL, 20 experiments total)

Pair	20,000 molec./mL		30,000 molec./mL		Z	Z-test conf. (1- α)
	MPN	σ	MPN	σ		
1	18,528	0.076	28,995	0.078	4.120	0.9999
2	19,126	0.076	27,027	0.077	3.192	0.9980
3	17,354	0.076	25,954	0.077	3.717	0.9995
4	17,077	0.076	29,976	0.078	5.163	1.0000
5	15,183	0.077	30,357	0.078	6.330	1.0000
6	16,518	0.076	25,279	0.077	3.929	0.9999
7	17,948	0.076	38,315	0.079	6.898	1.0000
8	20,442	0.076	36,545	0.079	5.294	1.0000
9	18,013	0.076	33,205	0.079	5.592	1.0000
10	23,967	0.077	31,779	0.078	2.577	0.9900
Avg.	18,226	0.076	30,316	0.078	4.672	1.0000

Table 3

Numbers of total and positive or negative wells required by theory to achieve specific resolution levels in single-volume systems (with criteria of 95% confidence and 95% power).

Resolution, X-fold	Asymptotic limit for LLQ-X (# of positive wells needed)	Asymptotic limit for ULQ-X (# of negative wells needed)	fewest total wells for this limit	Fewest total wells at which this resolution is possible (# of positives needed for LLQ-X, # of negatives needed for ULQ-X)
5	5	3	32	21 (6, 3)**
3	13	3	131	36 (19, 3)**
2	39	3	473	85 (55, 8)
1.5	130*	3	2110*	245 (179, 34)**

* Technically 129 wells is the asymptotic limit, but requires >80,000 total wells, so we use 130 positive wells instead.

** The ULQ-X is X-fold higher than LLQ-X

Table 4

Five designs at constant total well number and total volume that demonstrate the impact of changing VS on dynamic range.

VS	Design parameters				
	10	8	5	2	1
Design	1	2	3	4	5
Well # per volume	160	160	160	160	640
Well Volumes (nL)	140, 14, 1.4, 0.14	136, 17, 2.125, 0.2656	125, 25, 5, 1	83, 41.5, 20.75, 10.375	39
Total Volume (μL)	24.89	24.86	24.96	24.90	24.96
LDL (molec./mL)	121	121	120	120	120
ULQ (molec./mL)	2.840×10^7	1.497×10^7	3.976×10^6	3.833×10^5	1.375×10^5
Dynamic range (Log(ULQ/LDL))	5.4	5.1	4.5	3.5	3.1